Eur. Phys. J. Plus (2023) 138:407
https://doi.org/10.1140/epjp/s13360-023-03950-1

THE EUROPEAN PHYSICAL JOURNAL PLUS

Regular Article

Photocatalytic and antibacterial properties of pure and niobium-doped copper oxide nanoparticles

Gurdev Preet Singh, K. J. Singh[a]

Department of Physics, Guru Nanak Dev University, Amritsar, Punjab 143005, India

Received: 26 November 2022 / Accepted: 4 April 2023

Abstract Nb_2O_5 doped CuO nanoparticles (NPs) were prepared via simple ball milling technique. CuO nanoparticles doped with 0 (NB-0), 1 (NB-1) and 3 (NB-3) wt % of Nb_2O_5 were ball milled for 48 h. and then heated for 6 h. at 600 °C. Different characterization techniques were used for the investigation of structural and optical properties of Nb_2O_5 doped CuO nanoparticles. X-ray diffraction patterns of synthesized samples confirmed the monoclinic phase of the CuO with successful doping of Nb_2O_5 in host matrix. Unit cell volume and lattice parameters of NPs show complete dependency on the concentration of Nb_2O_5. Vibrational properties of the CuO nanoparticles were evaluated by FTIR spectrometer. UV–Visible spectroscopy data were used to evaluate the optical band energy of the samples. Photocatalytic behavior of nanoparticles was studied. 5 mg powder of each catalyst (NB-0, NB-1 and NB-3) was separately dispersed in 250 ml dye aqueous solution (10 g/1L). The mixture solution was stirred magnetically in dark for 1 h before photocatalytic test. Furthermore, the sample NB-3 (3 wt %) shows fastest and maximum rate of photocatalytic degradation of methylene blue dye among all the samples. The highest photocatalytic efficiency is obtained by NB-3 at (75%) as compared to NB-1 at (71.0%) and NB-0 at (67.5%). It is observed that almost complete degradation of Methylene Blue (MB) dye occurred under UV-light radiance within 150 min. Photocatalytic effect was due to interfacial charge transfer and reduced recombination rate of charge-carriers. The antibacterial activities of Nb_2O_5 doped CuO NPs against *Escherichia coli* and *Staphylococcus aureus* were explored in culture media by agar diffusion method. The experiment confirms that Nb_2O_5 doped CuO nanoparticles have the potential to degrade the organic pollutants and they have good candidature for becoming agents for bacteria inactivation. Also, enhancement is observed in antibacterial and degradation activity by increasing doping concentration. Moreover, authors report better photocatalytic activity against MB dye as well as better zone of inhibitions against E. Coli bacteria by employing niobium-doped copper oxide nanoparticles.

1 Introduction

The waste water released by the industries has become a foremost environmental concern all around the globe due to the presence of hazardous organic dyes which contaminate the water and also these are unsafe for ecosystem [1–3]. The synthetic dyes are released into open water; these dyes are hard to eliminate by traditional treatment methods due to their stable nature. Even at very low concentration, these dyes are harmful to both human and aquatic life. Hence, the effective removal of organic dye stuffs has readily become the main focus of research in the field of environmental remediation. At present, there are lot of techniques for implementation of waste management but there is need for more techniques due to expansion of industries at fast rate and urbanization [4, 5]. Among numerous range of purification techniques, heterogeneous photo-catalysis is the promising technology for environmental purification [6]. In recent trend the use of metal oxides is in demand for photocatalytic degradation. The different types of metal oxides used for this purpose include TiO_2, SnO_2, Fe_2O_3, CeO_2, ZnO, etc. The excellent metal oxides among these give good results under the exposure of UV light, owing to their wide band gap [7, 8]. This also has led to demand of the suitable dopant choice for formation of metal oxide composite and heterojunction for tuning of band gap in order to prepare photocatalysts [7–9]. Moreover, ability of the photocatalyst to adsorb organic pollutant and reduce the rate of charge carrier recombination would further improve its photocatalytic activity [10]. As an important semiconductor metal oxide with a narrow band gap (1.2–1.5 eV), copper oxide (CuO) has drawn attention in research field due to its attractive properties like chemical stability, electrochemical activity, excellent reactivity, low production cost, nontoxicity and abundant availability and has wide range of applications like super capacitors, solar cells, gas sensors, Li-batteries, super capacitors and catalysis [11–15]. There are limited reports on the photodegradation of organic dyes using CuO as photocatalyst because activity of pure CuO is not high enough due to the fast recombination rate of photogenerated electron–hole pairs [16–22]. To overcome this drawback, one possible solution is to dope CuO with another metals,

[a] e-mail: kanwarjitsingh.phy@gndu.ac.in (corresponding author)

Published online: 13 May 2023

non-metals, and semiconductor materials [23–25]. Doping has collective advantages of both semiconductor materials and further improves the separation of electron–hole pairs by keeping the reduction and oxidation reactions apart and enhances photocatalytic activity [26, 27]. Based on the above given facts, in this study, we have coupled CuO with Nb_2O_5 with the aim of achieving enhanced photocatalytic activity toward organic dyes. Niobium pentoxide (Nb_2O_5) has many interesting properties which are desirable for the photocatalytic degradation such as specific surface area and higher stability, band gap between 3.1 and 4.0 eV, and high absorption coefficient [28]. On other hand, one of the innovative methods presented against the bacterial resistance is the use of metal and oxide nanoparticles, heterostructures and nanocomposites [29, 30]. Metal oxides such as copper oxide (CuO) have special physicochemical properties arising due to quantum size effect and high specific surface area, which enhance the biological and chemical activity of the material [31, 32]. Another important property is the ability to target various types of bacterial structures. Selective permeability and the process of cellular respiration which are normal function of cell membrane are disrupted by these materials. In addition, these particles, after entering the bacterial cell, interfere with the function of proteins which contain sulfur and phosphate molecules such as DNA, and irradiate their function [33, 34]. The antibacterial activity of ZnO/Nb_2O_5 nanocomposite against various bacteria has been observed by Rakesh et al. [35]. Yi-Hao Pai and Su-Yun Fang have prepared porous Nb_2O_5 photocatalysts with CuO, NiO for hydrogen production by light-induced water splitting [36]. Saviz Zarrin and Felora Heshmatpour made new composites TiO_2/Nb_2O_5/PANI and TiO_2/Nb_2O_2/RGO for degradation of organic pollutants [37] Madhavi et al. studied the impact of Nb_2O_5on *in-vitro* bioactivity and antibacterial activity of CaF_2–CaO–B_2O_2–P_2O_2–SrO glass system [38]. In recent years, several methods have been introduced for the synthesis of metal oxide nanoparticles such as sol–gel [39], thermal oxidation [40], ball milling [39], combustion [41], and quick precipitation [42, 43]. Among all these various proposed methods for the synthesis of metal oxide nanoparticles, ball milling method is most easiest and economical method.

In present study we used ball milling method for synthesis of CuO-Nb_2O_5 NPs. XRD, SEM, Raman spectroscopy, DLS and UV–Visible spectroscopy techniques were utilized for evaluating structural, morphological, vibrational and optical properties. The photocatalytic activity against Methylene Blue (MB) dye and antibacterial activity against pathogens (*Escherichia coli* and *Staphylococcus aureus)* are also studied. To the best of our knowledge, no research work has been reported on the antibacterial and photocatalytic degradation of methylene blue dye by Nb_2O_5 loaded CuO NPs earlier.

2 Experimental method

2.1 Preparations of CuO-Nb_2O_5 nanoparticles

Samples were synthesized using traditional solid state reaction method, i.e., ball milling method. All the chemicals used were of analytic grade of purity. In a typical synthesis, CuO was mixed with 0, 1 and 3 wt% of Nb_2O_5 in distilled water and ball milled for 48 h. The samples were then dried overnight in oven at 80^0 C and then crushed properly to obtain fine powder. After that, the powdered samples were heated in muffle furnace at 600 °C for 6 h. The samples with wt % 0, 1 and 3 of Nb_2O_5 were labeled as NB-0, NB-1 and NB-3, respectively.

2.2 Photocatalytic activity

Photocatalytic activity of the synthesized nanoparticles was explored by studying the degradation of methylene blue dye under irradiation of UV-light. In this experiment, standard stock solution was prepared using D.I. water with concentration of 10 mg dye in 1 L. Each prepared sample was dispersed in 250 ml of MB dye solution. Then each beaker containing sample was stirred magnetically for 35 min in dark place to achieve equilibrium between photocatalyst and MB dye. Further, the suspensions were illuminated under UV-light for 180 min with continuous stirring. At each particular time interval, 5 ml of suspension was collected and centrifuged to extract the catalyst. The supernatant was then examined by UV–vis spectroscopy.

2.3 Photocatalytic-degradation procedures

All photocatalytic reactions were carried out under similar condition in a self-designed wooden box. This model consists of six UV lamps (Philips TUV 15W G15T8) that especially emit at 254 nm with exact power of 15W. All UV lights were installed in parallel keeping distance of 50 cm above the top surface of dye solution. Box was covered with black paper to prevent leakage of UV radiation. Magnetic stirrer for each sample was placed in center of box below UV light.

2.4 Antibacterial studies

Antibacterial activity of CuO-Nb_2O_5 nanoparticles was examined against E.coli and S.aurues bacteria by Agar well diffusion method. Activity of the samples NB-0, NB-1 and NB-3 against both the bacterial strains were calculated by zone of inhibition (ZOI). 0.1 ml E.coli and S.aurues suspension was taken from the prepared inoculum and distributed uniformly on the medium in petri dish. Then petri dishes were incubated for 26 h at 38 °C. After 24 h. period, 6 mm diameter wells were made in agar plates with the help of

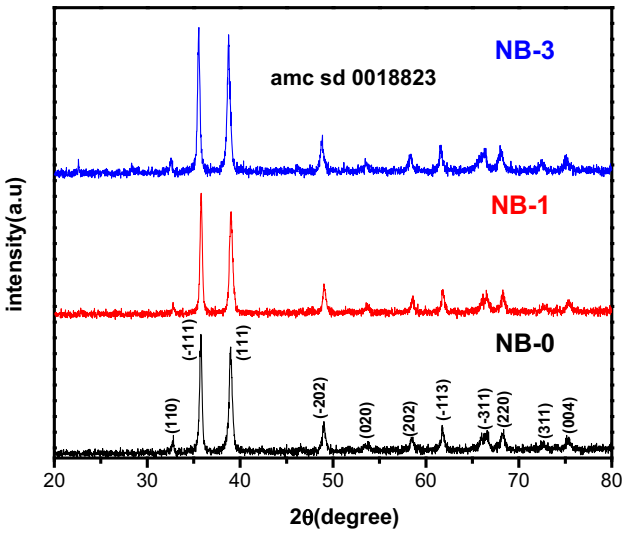

Fig. 1 X-ray diffraction patterns of pure and Nb_2O_5 doped CuO nanoparticles

cork-borer. Samples were added into wells by using micropipette. Petri dishes were incubated in BOD incubator for 48 h. for 3 days. Further, diameter of zone of inhibition produced by synthesized NPs including well size was measured.

2.5 Characterization

The synthesized CuO-Nb_2O_5 nanoparticles were characterized using variety of analytical instruments. Structural properties of Nano powders were examined using X-ray diffractometer, Shimadzu 7000 having scan speed of 2 degree per minute. Surface morphology of the samples was analyzed using Field Emission Scanning Electron Microscopy (FESEM) of ZEISS SUPERA 55. Jasco 460 Plus FTIR spectrometer was used to investigate the vibrational properties of the Nano-powders. Particle size distribution of the CuO nanostructures was obtained by a dynamic light scattering spectrometer (Malvern Zetasizer, Nano ZS90, UK). Optical properties of CuO-Nb_2O_5 nanoparticles were analyzed with the help of Cary 5000 UV Visible NIR spectrophotometer. Photocatalytic degradation of MB dye was recorded by Shimadzu UV-2450 spectrophotometer.

3 Results and discussions

3.1 X-ray diffraction studies

Figure 1 represents the X-ray diffraction pattern of CuO-Nb_2O_5 nanoparticles at room temperature. The sharp peaks in the graph show fine quality and polycrystalline character of all synthesized samples. All the diffraction peaks (110), (− 111), (111), (-202), (020), (202), (− 113), (− 311), (220), (311) and (004) are in correlation with planes of monoclinic CuO crystal structure and are in complete agreement with amc sd 0018823 card. There is no impurity peak seen in the pattern which confirms that dopant is successfully incorporated in the host matrix. Unit cell volume (V) and lattice constants (a, b, and c) of monoclinic CuO structure are evaluated by given equations.

$$\frac{1}{d^2} = \frac{1}{sin^2\beta}\left[\frac{h^2}{a^2} + \frac{k^2 sin^2\beta}{b^2} + \frac{l^2}{c^2} - \frac{2hlcos\beta}{ac}\right] \tag{1}$$

$$V = abcsin\beta \tag{2}$$

Inter-plane spacing d is calculated using Bragg's diffraction law. Miller indices are denoted by (hkl) and 99.54° is the value of lattice angle β. Calculated values for CuO structures are presented in Table 1 [44, 45]. Smaller ionic radius of dopant (0.63 A°) as compared to the Cu ions (0.73 Å) [3] is the main cause for decrease in the values of lattice parameters and unit cell volume of the CuO nanostructures. The micro-structural parameters such as crystallite size (D) and microstrain (ε) for the synthesized samples have been calculated using the following relations [46]

$$D = \frac{k\lambda}{\beta\cos\theta} \tag{3}$$

$$\varepsilon = \frac{\beta\cos\theta}{4} \tag{4}$$

Table 1 Lattice parameters (a,b and c), unit cell volume (V), crystallite size (D), strain(ε) and energy band gap (E_g) of CuO pure and Nb_2O_5 doped nanoparticles

Sample name	Structural parameters of CuO				Crystallite size	Strain	E_g (eV)
	a (Å)	b (Å)	c (Å)	V(Å^3)	D (nm)	$\varepsilon \times 10^{-3}$	
NB-0	4.655	3.415	5.062	79.37	26.50	3.6	5.64
NB-1	4.662	3.418	5.224	82.10	29.84	4.1	5.40
NB-3	4.668	3.420	5.233	82.40	33.60	6.0	5.10

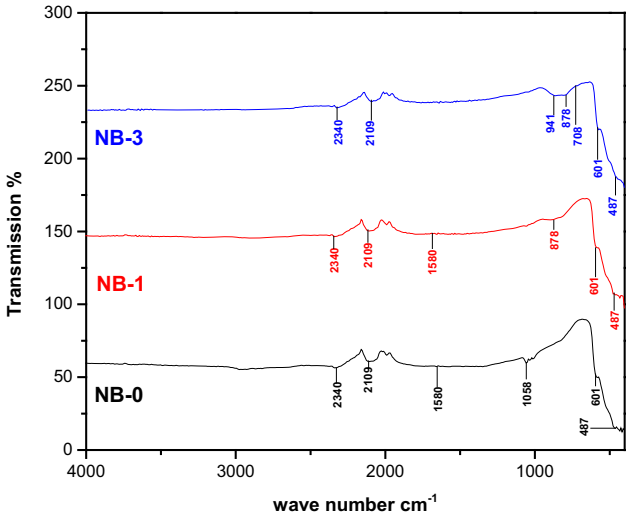

Fig. 2 FTIR spectra of pure and Nb_2O_5 doped CuO nanoparticles

where λ (1.54 Å) is the wavelength of the X-Rays, k (0.89) is a constant and β is full width at half maximum (FWHM). The average crystallite size of CuO has been found to increase with the increasing concentration of Nb_2O_5. The calculated values of crystallite size and microstrain are given in Table 1. The agglomeration process between CuO and Nb_2O_5 in the nanocomposite results in an increase of the grain size due to the difference between their atomic radii. Calculated microstructural parameters are similar to [34]. The microstrain values increase with Nb_2O_5 content, due to the higher effect of grain size on the comprehensive stress of the nanocomposite.

3.2 FTIR studies

FTIR-spectra of all synthesized samples are displayed in Fig. 2. The spectrum of sample NB-0 shows no other active mode between 600 and 605 cm^{-1} which completely exclude the presence of any other phase like Cu_2O.The other peaks 2340 cm^{-1}, 2109 cm^{-1}, 1580 cm^{-1} and 1058 cm^{-1} refer to the O–H bond deformation and elongation vibration and also reveals the presence of H_2O. Peak at 601 cm^{-1} shows Bu mode of CuO which is high frequency mode and represent elongation of the Cu–O bond. On the other hand, the peak at 495 cm^{-1} is due to the deformation vibrations of the Cu–O bond. In spectra of sample NB-1, peak at 878 cm^{-1} can be attributed to Nb = O stretching. Peaks at 901 cm^{-1} and 708 cm^{-1} of spectrum NB-3 represent bending and stretching vibrations of Nb–O [47–51].

3.3 Optical properties

The optical properties of pure and Nb_2O_5 -doped CuO samples were analyzed to investigate the effect of doping on the band gap energy by UV–visible spectra. The spectra were recorded between 200 and 800 nm wave length region at room temperature. Figure 3a shows a strong fundamental absorption edge approximately 219 nm which is due to direct transition of electrons [52]. The optical band gap energy E_g of all the samples was estimated from plot between $(\alpha h\nu)^n$ and E_g as shown in Fig. 3. Tauc's relation was used for calculation of optical energy as per the following relation [3]:

$$(\alpha h\nu)^n = B(h\nu - E_g) \tag{5}$$

where α is the absorption coefficient, $h\nu$ photon energy having units in eV. 'n' is constant having allowed transition value up to 2 and B represents band tailoring constant. The estimated band gap values are 5.65, 5.40, and 5.10 eV for NB-0, NB-1 and NB-3, respectively, which is higher than bulk CuO (1.25 eV). In the literature various reports represent similar trends [53–56]. The bandgap of CuO nanoparticles decreases with an increase in doping concentration of Nb_2O_5.The decrease in bandgap may be due to transfer of charge between the conduction band of CuO and the impurity energy level of Nb_2O_5 [54]. This charge transfer might have

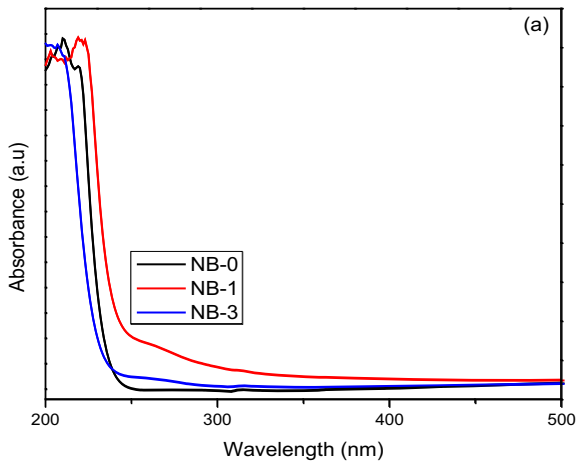

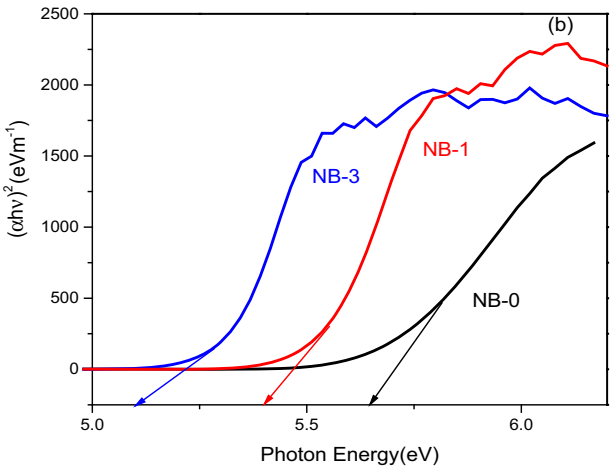

Fig. 3 **a** UV–visible absorption spectra of pure and Nb_2O_5 doped nanoparticles **b** Plot of $(\alpha h\nu)^2$ versus photon energy

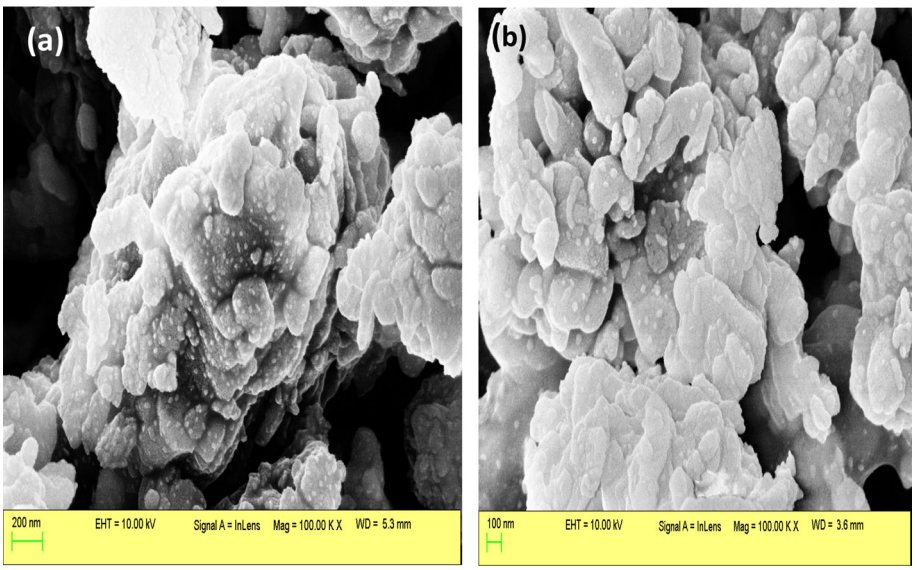

Fig. 4 FESEM images of **a** NB-0 **b** NB-3

produced trapping levels in the Nb_2O_5-doped CuO nanostructure which in result decreases the bandgap of CuO. Moreover, the reduction of band gap with the addition of dopant material induces transformation from valance to conduction band with less energy, which may encourage the photocatalytic activity and antibacterial properties in our study [54, 58, 59].

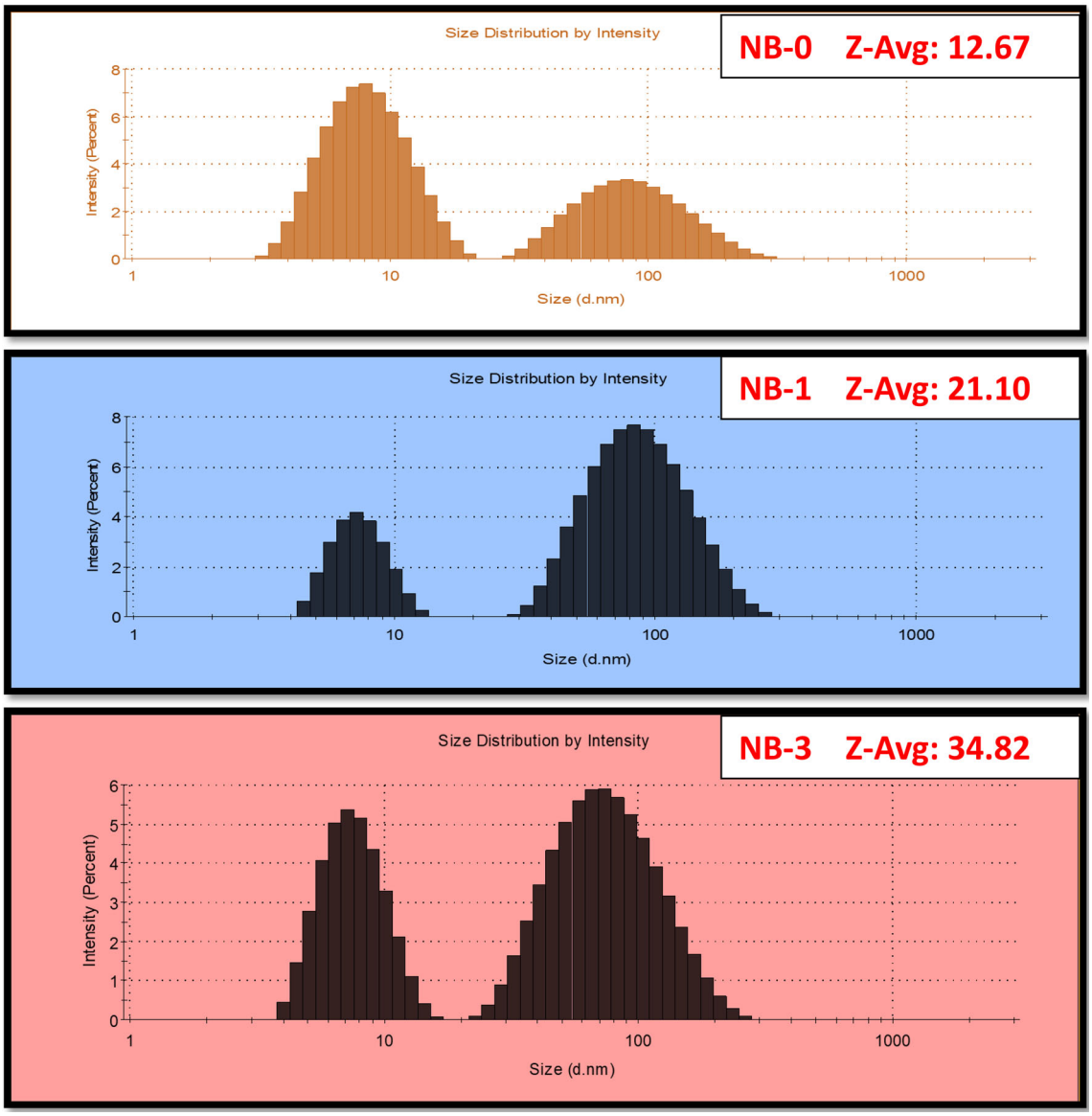

Fig. 5 Particle distribution plots of the samples obtained from DLS stud

3.4 Field emission scanning electron microscopy analysis of CuO-Nb_2O_5 nanoparticles

FESEM micrographs of samples NB-0 and NB-3 are shown in Fig. 4 which depicts the Nano flower-like structure of CuO pure and CuO doped Nb_2O_5 NPs. Morphology and crystallinity mainly depend upon rate of aggregation of the final output. Moreover in images, it is observed that nucleation and growth rate of CuO flower like structure increases by increasing concentration of dopant (Nb_2O_5) which further results in increased particle size, which is in complete agreement with the XRD results given in Table 1. [60, 61].

3.5 Dynamic light scattering studies

The information of particle size distribution is obtained from the dynamic light scattering (DLS) analyzer. The samples were dispersed in distilled water and DLS studies were carried out at room temperature [62, 63]. The particle size distributions of the samples obtained from DLS measurements are shown in Fig. 5. The obtained values of particle size indicate that the average size of the nanoparticles increases with the increase in dopant concentration; similar results are reported in literature [64]. The average particle size of doped nanoparticles was found in agreement with average size given in literature [65]. Moreover, average particle size of the samples obtained from DLS measurements is in good agreement with XRD results.

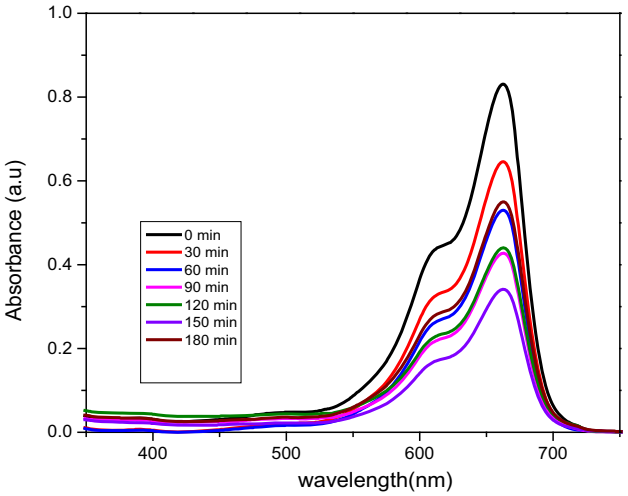

Fig. 6 Absorption spectra of MB dye in the presence of NB-0

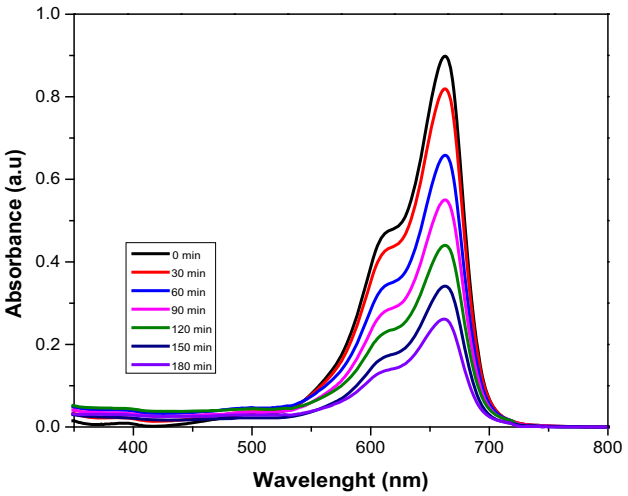

Fig. 7 Absorption spectra of MB dye in the presence of NB-1

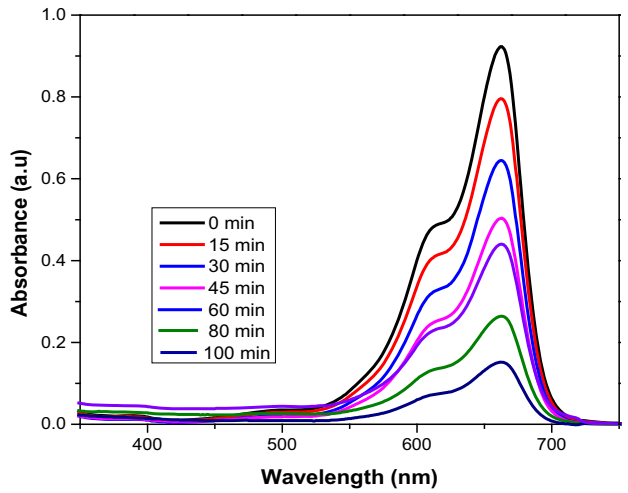

Fig. 8 Absorption spectra of MB dye in the presence of NB-3

3.6 Photocatalytic activity of synthesized CuO-Nb_2O_5 nanoparticles

The photo-catalytic activities of synthesized CuO-Nb_2O_5 nanoparticles were evaluated against MB dye solution under UV-light radiance. The degradation efficiency (E) was calculated by the following equation

$$E = [(C_O - C_t)/C_o] \times 100 \quad (6)$$

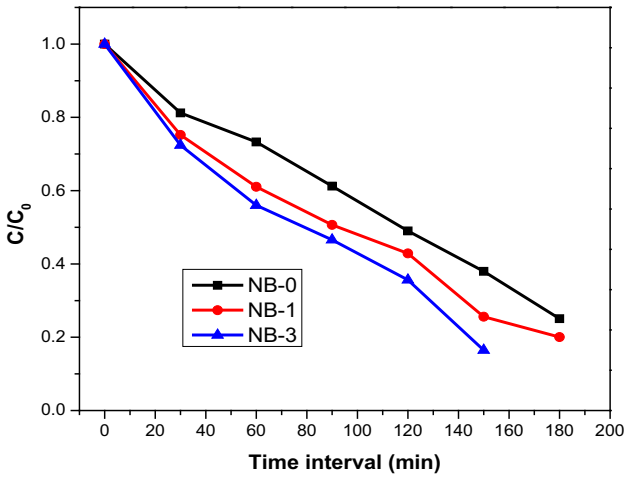

Fig. 9 Photo-catalytic efficiencies of synthesized samples NB-0, NB-1 and NB-3 in MB blue dye Degradation as a function of time

Table 2 Photo degradation kinetic parameters of synthesized CuO-Nb_2O_5 nanoparticles

Sample code	Degradation efficiency η (%)	Intercept(c)	Residual sum of squares	Pearson's (r)	R^2
NB-0	67.50	0.205	0.034	0.988	0.971
NB-1	71.10	0.209	0.001	0.995	0.988
NB-3	75.00	0.396	0.025	0.994	0.985

where C_t is the concentration of dyes at any time during photocatalysis reaction and C_O is the initial concentration at the start of the reaction. The photocatalytic activity of NB-0, NB-1 and NB-3 Nano-composites were assessed by photo-degradation of MB under UV-light irradiation as shown in Figs. 6, 7 and 8. When the aqueous solution of MB dye is irradiated for 180 min, the degradation of MB dye is found to be very low. MB was stable and very hard to decompose without photocatalyst. NB-3 composite sample was found to be more photoactive for photo degradation of MB dye as compared to NB-1 and NB-0 samples. The degradation rate follows as CuO-Nb_2O_5 (3%)>CuO-Nb_2O_5 (1%)>CuO (0%). Degradation of the samples with varying time is shown in Fig. 9. The photocatalytic degradation efficiency of MB was found to be 75% for NB-3, 71.10% for NB-1 and 67.50% for NB-0. In general, during UV exposure, electron hole pairs are formed due to movement of electrons from valence band to conduction band and holes are left behind in valence band. The generated electron–hole pairs lead to oxidation and reduction processes and create hydroxyl radicals and superoxide anions. In this study, the presence of dopant restricts the electron–hole pair recombination by introducing an impurity level between conduction band and valence band of host material. The pseudo-first-order kinetic model was used to evaluate the performance of photo-catalyst as [47, 66]:

$$C_t = C_0 e^{-kt} \tag{7}$$

$$ln(C_0/C_t) = kt \tag{8}$$

where k is photocatalytic degradation rate constant, C_t is the temporal concentration of MB dye, C_0 is the initial concentration of the MB dye and t is the degradation reaction time. The values of R^2 and all other parameters related to degradation are presented in Table 2. R^2 value near one indicates good linear fitting of data and therefore, it is concluded that all the samples NB-0, NB-1 and NB-3 follow pseudo-first-order kinetic the degradation rate constant, k increases by increasing dopant concentration, confirming that the sample NB-3 is more effective than all other samples in removal of MB dye. The improved photocatalytic activity may be attributed to following reasons (1) Structural defects created by dopant (2) Interstitial sites favoring the degradation process (3) Retardation in recombination rate of electron–hole pairs [67–69]. A proposed mechanism for photocatalytic degradation of MB under UV light is shown in Fig. 10. Initially, dye degradation is determined by color change. At start of the experiment, the color of dye shows deep blue color then it changes to light blue color within time period of 30–50 min in the presence of catalyst. Thereafter, light blue color changes to light green. This change in color of dye solution from initial deep blue color to colorless is shown in Fig. 11. In comparison, our results show better degradation rate of Methylene blue dye by CuO-Nb_2O_5 nanoparticles taking only 100 min to degrade MB dye up to 75%, whereas Sarvanan et al., which reveals 71.28% degradation of MB dye in 120 min for the sample ZnO/CuO (90:10).

E.coli and S.auereus bacteria were used as a model to test the in vitro antibacterial activity. The bactericidal activity against by both bacteria is shown in Fig. 12. Antibacterial activities are observed, without creating any colonies when the nanoparticles are in contact with the pathogens. The area which is created without colonies is called zone of inhibition [70, 71]. The observed results revealed that there is increase in antibacterial activity by doping Nb_2O_5 which give rise to rise in zone of inhibition diameter. Till now, many mechanisms have been conferred for the antibacterial activity of metal oxide NPs against pathogens. Instead of having

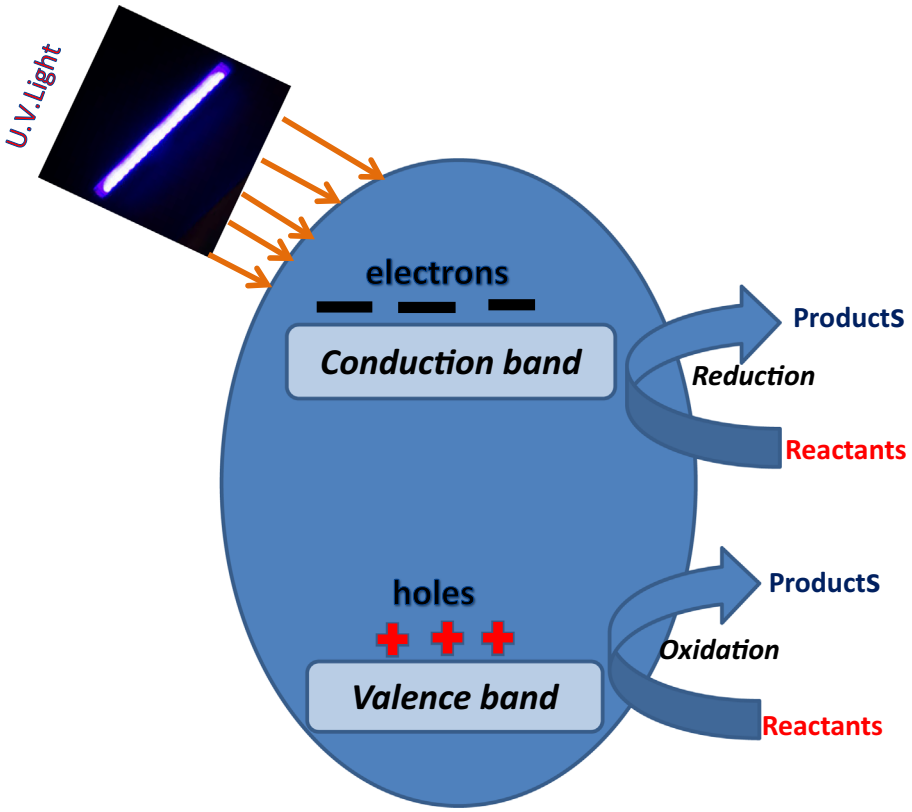

Fig. 10 Photocatalytic degradation of methylene blue dye by under sunlight Nb_2O_5 doped CuO nanoparticles

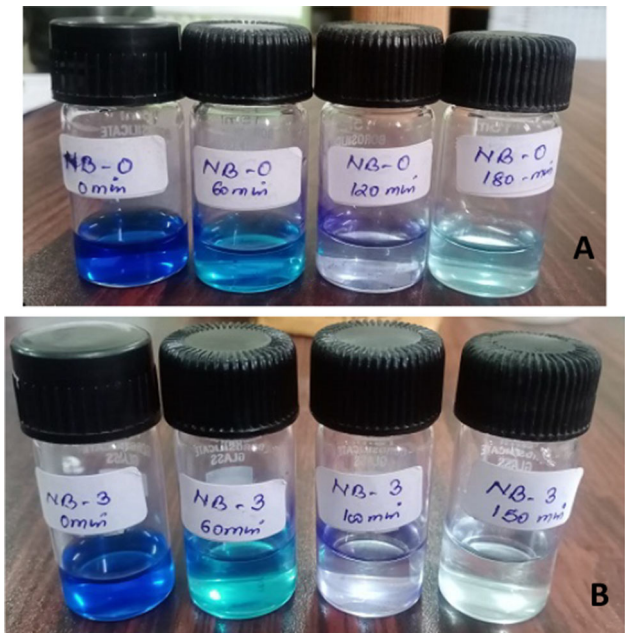

Fig. 11 Photo-catalytic degradation of methylene blue using **A** Synthesized CuO NPs **B** Synthesized Nb_2O_5 (3% wt) doped CuO NPs

so many studies still the mechanism is not properly clear. There are lot of factors which affect the toxicity of NPs such as intrinsic properties, strain of bacteria and surface morphology.

3.7 Antibacterial activity of synthesized CuO-Nb_2O_5 Nanoparticles

The first and simple phenomenon is that nanostructures battling against pathogens attach to their membrane and then pathogen and electrostatic attraction is induced due to which nanostructures are in contact with bacteria and rupture the cell wall [72, 73], which leads to death of bacteria. Second and most important mechanism is (ROS) generation by nanoparticles. Hydroxyl radicals

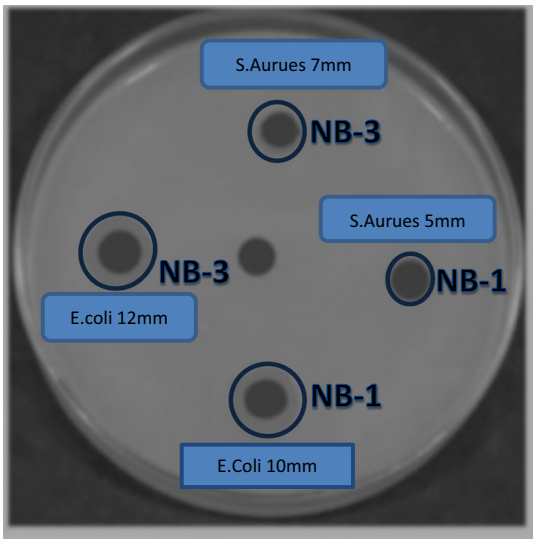

Fig. 12 Antibacterial activities of CuO-Nb_2O_5 nanoparticles

Table 3 Inhibition zone values of nanocomposites against S. Aureus and E.coli

Sample code	Concentration of samples mg/ml	Bacterial strain (Zone of Inhibition)	
	2, 5, 10	S. Aureus(mm)	E. Coli(mm)
NB-0		0	0
NB-1		5	10
NB-3		7	12

(OH^-), hydrogen peroxide (H_2O_2), superoxide anion radicals (O_2^-) and singlet oxygen ($^1O_2$) are all known as ROS. These ROS enter cytoplasm of pathogens and induce variation in activity of protein which leads to death of pathogens [74]. ROS radicals are generated when the metal oxide nanoparticles are in contact with molecules of the water. Defects in the crystal structures of metal oxide nanoparticles play an important role in the creation of ROS [75]. Doping another metal oxide as dopant in host metal oxide enhances the structural defects which further generate more ROS and improve antibacterial activity. In our study, possible mechanism involved in the antimicrobial activity can be attributed from the disruption of cell membrane due to the discharge of copper ions from CuO nanoparticles, which adhere to negatively charged bacterial cell wall and rupture it, thereby dominating protein denaturation and cell death [76–79]. As we increase Nb_2O_5 content, it increases defects and replaces more and more Cu^{2+} which results in higher antimicrobial activity. The less permeable nature of S.Aurues and E. coli gives a state way for the entry of Cu^{2+} ions and enhance rate of cell death [80]. Mechanism of antibacterial activity of nanoparticles is shown in Fig. 13 [81–83]. In this experiment, zone of inhibition was observed against both bacteria using different concentration of synthesized NPs as (2, 5 and 10 mg/ml). The data for zone of inhibition are given in Table 3. Highest antibacterial activity was observed by NB-3 sample against E.coli (ZOI-12 mm) at conc. 10 mg/ml. NB-2 showed lowest activity against S.auereus (ZOI-5 mm) at conc. 5 mg/ml. ZOI-10 mm against E.coli and ZOI-7 mm against S.auereus was shown by NB-2 and NB-3 at conc 0.10 mg/ml and 5 mg/ml, respectively. NB-1 sample shows negligible activity for pathogens at all concentration. Whereas NB-2 and NB-3 samples has shown negligible activity only for concentration of 2 mg/ml for both pathogens. It is observed that by increasing the concentration of dopant antibacterial activity increases [84–86]. The interaction in the antibacterial activity could be as following [87]

$$N + h\upsilon \rightarrow e^- + h^+ \tag{9}$$

$$e^- + O_2 \rightarrow O_2^{*-} \tag{10}$$

$$e^- + O_2^{*-} + 2H \rightarrow H_2O_2 \tag{11}$$

$$2e^- + HO_2^{*-} + H^+ \rightarrow OH^* + OH^- \tag{12}$$

In Eq. (6) N is shown as synthesized nanoparticles. During bacterial death mechanism among all ions, OH^* is examined as highest active ion. It is observed that antibacterial activity against S.aureus is more resisting than E.coli and this is based on biological structure of pathogens membrane cell wall chemical configuration. Rakesh et al. have also reported the antibacterial activity of Nb_2O_5 doped ZnO nanoparticles against *E. coli* bacteria [35]. They have reported the best activity of 1.9 mm (zone of inhibition) against the E. coli bacteria at 1 mg/ml dose concentration. Our sample doped show better antibacterial behavior (10 mm zone of inhibition) against *E. coli* bacteria at higher concentrations (2 mg/ml).

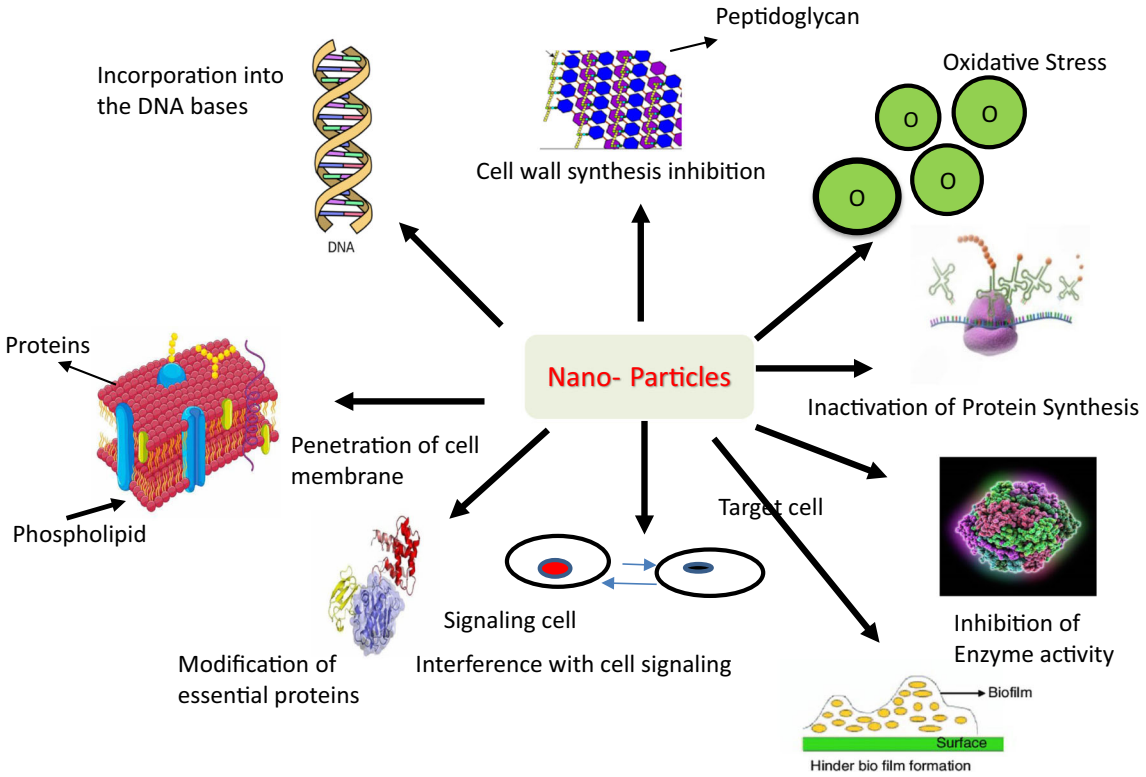

Fig. 13 Mechanism for antibacterial activity of nanoparticles

4 Conclusions

In summary, cost-effective CuO-Nb_2O_5 nanoparticles were successfully synthesized by ball milling technique. The Nb_2O_5 doped CuO NPs showed monoclinic phase of CuO with good crystalline quality peaks (110), (− 111), (111), (− 202), (020), (202), (− 113), (− 311), (220), (311) and (004) and no other secondary phase was seen in XRD data. By calculation, it is clear that dopant increases the size of unit cell volume by increasing concentration and this is also compatible with FESEM pictures for NB-0 and NB-3 samples. FESEM surface morphology reveals the development of CuO Nano-flowers in size. FTIR characterization proved the existence of the characteristic bands of copper oxide CuO and Nb_2O_5 bringing up the development of CuO-Nb_2O_5 NPs. In addition, synthesized CuO-Nb_2O_5 nanoparticles were used as catalyst for photocatalytic degradation of MB dye under UV-light radiation. The Nb_2O_5 doped CuO nanostructures exhibit excellent photo degradation of MB dye. NB-3 sample has shown almost complete degradation (75%) of MB dye under UV-light within 100 min, as compared to NB-0 sample which shown (67.5%) degradation in 180 min. The results confirmed that CuO catalytic was substandard compared to CuO-Nb_2O_5. The results of kinetic study confirm that all samples show the first-order linear kinetic. The optical band gap decreases with increasing the concentration of Nb_2O_5.which results in enhancement of photocatalytic and antibacterial activity. The antibacterial activity of synthesized NPs on E. coli and S. aureus proved that all doped samples could obstruct bacteria activity but depends upon the concentration of the samples. The antibacterial activity is directly proportional to the concentration of the samples. In present study, higher antibacterial activity is seen for E.coli as compared to S.aureus. To the best of our knowledge, Nb_2O_5 doped CuO NPs have not been used for antibacterial activity and MB dye degradation studies together. Our results show good degradation for MB dye and better antibacterial activity against E.coli than S.auereus bacteria. Moreover, based on above evidence, this research provides suitable material for wastewater treatment, biomedical fields and optical applications.

Acknowledgements Authors thank Department of Emerging Sciences, Guru Nanak Dev University-Amritsar, India for providing SEM, XRD and UV facility for this work. One of the authors, Gurdev Preet Singh like to give special thanks to Dr. Jasvir Singh for discussions and motivation, and Dr.Rajender Singh, SAIF, Panjab University-Chandigarh, India for providing TEM facility to complete this research work. In addition, authors thank Mr. Brhamjot Singh, Department of Pharmaceutical Sciences, Guru Nanak Dev University, Amritsar-Punjab, India for his excellent assistance to investigate antibacterial activities.

Data availability Data will be made available on request.

References

1. G. Cai, H. Luo, Li. Guo, L. Li, S. Zhang, MoOx -Si heterojunction with wide-band-gap MoOx contact layer in the application of low-intensity visible-light sensing. Mater. Sci. Semicond. Process. **131**, 105879 (2021)
2. A. George, D.M. Raj, A.D. Raj, A.A. Irudayaraj, J. Arumugam, H.J. Prabu, S.J. Sundaram, N.A. Al-Dhabi, M.V. Arasu, M. Maaza, K. Kaviyarasu, Temperature effect on CuO nanoparticles: antimicrobial activity towards bacterial strains. Surf Interf **21**, 100761 (2020)
3. L. Arun, C. Karthikeyan, D. Philip, D. Dhayanithi, N.V. Giridharan, C. Unni, Influence of transition metal ion Ni^{2+} on optical, electrical, magnetic and antibacterial properties of phyto-synthesized CuO nanostructure. Opt Quant Electr. **414**, 1–19 (2018)
4. C. Grégorio, L. Eric, Advantages and disadvantages of techniques used for Wastewater treatment. Environ Chem Lett **17**, 145–155 (2018)
5. P.R. Gogate, A.B. Pandit, A review of imperative technologies for Waste water treatment II: hybrid methods. Adv. Environ. Res. **8**, 553–597 (2004)
6. Y. Liu, L. Ren, X. Qi, Y. Wang, X. Liu, J. Zhong, One-step hydrothermal fabrication and enhancement of the photocatalytic performance of CdMoO4/CdS hybrid materials. RSC Adv. **4**, 8772–8778 (2014)
7. J. Yan, Y. Zhang, S. Liu, W. Guangjun, L. Li, N. Guan, J Mater Chem A **3**, 21434–21438 (2015)
8. C.L. Zhang, J.-J. Li, S.-Y. Li, Mater. Lett. **206**, 146–149 (2017)
9. Y.G. Habba, M. Capochichi-Gnambodoe, Y. Leprince-Wang, Appl. Sci. **7**, 1185 (2017)
10. A. Kubiak, K. Siwinska-Ciesielczyk, Z. Bielan, A. Zielinska-Jurek, T. Jesionowski, Adsorption **25**, 309–325 (2019)
11. Yi. Lin, P. Ren, C. Wei, Cryst Eng Comm **21**, 3439–3450 (2019)
12. J. Li, W. Nianqiang, Catal. Sci. Technol. **5**, 1360–1384 (2015)
13. C. Yang, X. Su, J. Wang, X. Cao, S. Wang, L. Zhang, Facile microwave-assisted hydrothermal synthesis of varied-shaped CuO nanoparticles and their gas sensing properties. Sens. Actuat. B **185**, 159–165 (2013)
14. R.P. Wijesundera, Fabrication of the CuO/Cu2O heterojunction using an electrodeposition technique for solar cell applications. Semicond. Sci. Technol. **25**, 045015 (2010)
15. Y.M. Juan, H.T. Hsueh, T.C. Cheng, C.W. Wu, S.J. Chang, Electron-field-emission enhancement of CuO Nanowires by UV illumination. ECS Solid State Lett. **3**, P30–P32 (2014)
16. C. Wang, J. Xu, R. Ma, M.F. Yuen, Facile synthesis of CuO nanoneedle electrodes for high-performance lithium-ion batteries. Mater. Chem. Phys. **148**, 411–415 (2014)
17. S.E. Moosavifard, J. Shamsi, S. Fani, S. Kadkhodazade, Facile synthesis of hierarchical CuO nanorod arrays on carbon nanofibers for high-performance supercapacitors. Ceram. Int. **40**, 15973–15979 (2014)
18. F. Gao, H. Pang, S. Xu, Q. Lu, Copper-based nanostructures: promising antibacterial agents and photocatalysts. Chem. Commun. (2009). https://doi.org/10.1039/b904801d
19. J. Li, F. Sun, K. Gu, T. Wu, W. Zhai, W. Li, S. Huang, Preparation of spindly CuO micro-particles for photodegradation of dye pollutants under a halogen tungsten lamp, Appl. Catal., A 406,51–58 (2011)
20. M.U. Anu Prathap, B. Kaur, R. Srivastava, Hydrothermal synthesis of CuO micro-/nanostructures and their applications in the oxidative degradation of methylene blue andnon-enzymatic sensing of glucose/H_2O_2. J Coll Interf Sci **370**, 144–154 (2012)
21. M. Rabbani, R. Rahimi, M. Bozorgpour, J. Shokraiyan, S.S. Mogha, Photocatalytic application of hollow CuO microspheres with hierarchical dandelion-like structures synthesized by a simple template free approach. Mater. Lett. **119**, 39–42 (2014)
22. B. Shaabani, Ebrahim Alizadeh-Gheshlaghi, Yashar Azizian-Kalandaragh, Ali Khodayari, Preparation of CuO nanopowders and their catalytic activity in photodegradation of Rhodamine-B, Adv. Powder Technol. 25 ,1043–1052(2014) Ahmad M, Ahmed E, Zhang Y, Khalid N, Xu J, et al.,Preparation of highly eicient Al-doped ZnO photocatalyst by combustion synthesis. Curr Appl Phys 13: 697–704 (2013)
23. M. Ahmad, E. Ahmed, Y. Zhang, N.R. Khalid, J. Xu, M. Ullah, Z. Hong (2013) Preparation of highly efficient Al-doped ZnO photocatalyst by combustion synthesis. Curr. Appl. Phys. 13(4):697–704. https://doi.org/10.1016/j.cap.2012.11.008
24. S. Liu, C. Li, J. Yu, Q. Xiang, Improved visible-light photocatalytic activity of porous carbon self-doped ZnO nanosheet-assembled lowers. Cryst Eng Comm **13**, 2533–2541 (2011)
25. K. Vignesh, A. Suganthi, M. Rajarajan, S. Sara, Photocatalytic activity of AgI sensitized ZnO nanoparticles under visible light irradiation. Powd Technol **224**, 331–337 (2012)
26. A. Sadollahkhani, Z.H. Ibupoto, S. Elhag, O. Nur, M. Willander, Photocatalytic properties of different morphologies of CuO for the degradation of congo red organic dye. Ceram. Int. **40**, 11311–11317 (2014)
27. J. Yang, Z. Li, W. Zhao, C. Zhao, Y. Wang, X. Liu, Controllable synthesis of Ag-CuO composite nanosheets with enhanced photocatalytic property. Mater. Lett. **120**, 16–19 (2014)
28. Y.J. Chiang, C.C. Lin, Photocatalytic decolorization of methylene blue in aqueous solutions using coupled ZnO/SnO_2 photocatalysts. Powder Technol. **246**, 137–143 (2013)
29. Q. Wang, S. Yu, Z. Tan, R. Zhang, Z. Li, X. Gao, B. Shen, H. Su, Synthesis ofmonodisperse Bi_2O_3-modified CeO_2 nanospheres with excellent photocatalytic activity under visible light. CrystEngComm **17**, 671–677 (2015)
30. O.F. Lopes, V.R. Mendonça, F.B.F. Silva, E.C. Paris, C. Ribeiro, Óxidos de nióbio: uma visão sobre a síntese do Nb_2O_5 e sua aplicação em fotocatálise heterogênea. Quím. Nova **38**, 106–117 (2015)
31. A.M. Allahverdiyev, K.V. Kon, E.S. Abamor, M. Bagirova, M. Rafailovich, Expert Rev. Anti-Infect. Ther. **9**, 1035–1052 (2011)
32. Z. Guo, Nanomedicine **14**, 1800 (2018)
33. Z. Guo, X. Liang, T. Pereira, R. Scaffaro, H. Thomas Hahn, Compos. Sci. Technol. **67**, 2036–2044 (2007)
34. N. Wu, D. Xu, Z. Wang, F. Wang, J. Liu, W. Liu, Q. Shao, H. Liu, Q. Gao, Z. Guo, Carbon **145**, 433–444 (2019)
35. Rakesh, S. Ananda, NM. Made Gowda, KR Raksha, Synthesis of niobium doped ZnO nanoparticles by electrochemical method: characterization, photodegradation of indigo carmine dye and antibacterial study. Adv Nanopart, **3**:133–147 (2014)
36. Y.-H. Pai, S.-Y. Fang, Preparation and characterization of porous Nb_2O_5 photo catalysts with CuO, NiO and Pt cocatalyst for hydrogen production by light-induced water splitting. J. Power Sources **230**, 321–326 (2013)
37. S. Zarrin, F. Heshmatpour, Photocatalytic activity of TiO_2/Nb_2O_5/PANI and TiO_2/Nb_2O_5/RGO as new nanocomposites for degradation of organic pollutants. J Hazard Mater **351**, 147–159 (2018)
38. B. Madhavi, A. Siva Sesha Reddy, P. Syam Prasad, A. Prasad, P. Pavani Koteswari Devi, V. Ravi Kumar, N. Veeraiah, The impact of Nb_2O_5 on in-vitro bioactivity and antibacterial activity of CaF_2-CaO-B_2O_3-P_2O_5-SrO glass system. Ceram Int **278**, 125653 (2021)
39. M.E. Grigore, E.R. Biscu, A.M. Holban, M.C. Gestal, A.M. Grumezescu, Pharmaceuticals **9**, 75 (2016)
40. M. Kaur, K. Muthe, S. Despande, S. Choudhury, J. Singh, N. Verma, S. Gupta, J. Yakhmi, J. Cryst. Growth **289**, 670–675 (2006)
41. M. Yamukyan, K.V. Manukyan, S. Kharatyan, Chem. Eng. J. **137**, 636–642 (2008)
42. R. Wu, Z. Ma, Z. Gu, Y. Yang, J. Alloys Compd. **504**, 45–49 (2010)

43. J. Zhu, D. Li, H. Chen, X. Yang, L. Lu, X. Wang, Mater. Lett. **58**, 3324–3327 (2004)
44. J. Singh, S. Sharma, S. Soni, S. Sharma, R.C. Singh, Mat Sci Semicon Proc **98**, 29–38 (2019)
45. R.O. Yathisha, Y. Arthoba Nayaka, P. Manjunatha, H.T. Purushothama, M.M. Vinay, K.V. Basavarajappa, Physica E **108**, 257–268 (2018)
46. H.M. Cakmak, H.A. Cetinkara, S. Kahraman, Super Latt. Microstr. **51**, 421–429 (2012)
47. E.F. Abo, I.A. Zeid, A.M. Ibrahem, W.A.A. Ali-Mohamed, The effect of CdO content on the crystal structure, surface morphology, optical properties and photocatalytic efficiency of p-NiO/n-CdO nanocomposite. Results Phys. **12**, 562–570 (2019)
48. A.G.S. Prado, L.B. Bolzon, C.P. Pedroso, A.O. Moura, L.L. Costa, Nb_2O_5as efficient and recyclable photocatalyst for indigo carmine degradation. Appl. Catal. B-Environ.-Appl. Catal. B-Environ. **82**, 219–224 (2008)
49. S. Roguai, A. Djelloul, A simple synthesis of CuO NPs for photocatalytic applications and theirs structural and optical properties. J New Technol Mater **11**, 53–57 (2021)
50. F. Mukhtar, T. Munawar, M.S. Nadeem, M. Hasan, F. Hussain, M. Asif-Nawaz, F. Iqbal, Multi metal oxide NiO-Fe_2O_3-CdO Nano composite-synthesis, photocatalytic and antibacterial properties. Appl. Phys. A **126**, 588 (2020)
51. S. Thakur, M. Shandilya, S. Thakur, D.K. Sharma, Growth mechanism and characterization of CuO nanostructure as a potent Antimicrobial agent. Surf. Interf. **20**, 100551 (2020)
52. N.R. Dhineshbabu, V. Rajendran, N. Nithyavathy, R. Vetumperumal, Study of structural and optical properties of cupric oxide nanoparticles. Appl Nanosci **6**, 933–939 (2015)
53. K. Mageshwari, R. Sathyamoorthy, J. Yong, L.J. Park, Novel $CuCr_2O_4$ embedded CuO nanocomposites for efficient photodegradation of organic dyes. Appl. Surf. Sci. **353**, 95–102 (2015)
54. S. Jimkeli Singh, P. Chinnamuthu, Highly efficient natural-sunlight-driven photodegradation of organic dyes with combustion derived Ce-doped CuO nanoparticles. Coll. Surf. A: Physicochem. Eng. Aspects **625**, 126864 (2021)
55. S. Ghazal, N. Khandannasab, H. Ali Hosseini, Z. Sabouri, A. Rangrazi, M. Darroudi, Green synthesis of copper-doped nickel oxide nanoparticles using okra plant extract for the evaluation of their cytotoxicity and photocatalytic properties. Ceram. Int. **47**, 27165–27176 (2021)
56. A.T. Babu, R. Antony, Green synthesis of silver doped nano metal oxides of zinc and copper for antibacterial properties, adsorption, catalytic hydrogenation and photodegradation of aromatics. J. Environ. Chem. Eng. **7**(1), 102840 (2018)
57. A.A. Menazea, M.K. Ahmed, Silver and copper oxide nanoparticles-decorated graphene oxide via pulsed laser ablation technique: preparation, characterization, and photoactivated antibacterial activity. Nano-Struct. Nano-Objects **22**, 100464 (2020)
58. S.F. Mansour, S.I. El-dek, M.K. Ahmed, Tailoring the structure of biphasic calcium phosphate via synthesis procedure. Mater. Res. Expr. **4**(12), 5015 (2017)
59. S.F. Mansour, S.I. El-Dek, M.K. Ahmed, Physico-mechanical and morphological features of zirconia substituted hydroxyapatite nano crystals. Sci. Rep. **7**, 43202 (2017)
60. S.A. Khan, S. Shahid, S. Hanif, H.S. Almoallim, S.A. Alharbi, H. Sellami, Green synthesis of chromium oxide nanoparticles for antibacterial, antioxidant anticancer, and biocompatibility activities. Int. J. Mol. Sci. **22**, 502 (2021)
61. S. Ghazal, A. Akbari, H.A. Hosseini, Z. Sabouri, F. Forouzanfar, M. Khatami, M. Darroudi, Biosynthesis of silver-doped nickel oxide nanoparticles and evaluation of their photocatalytic and cytotoxicity properties. Appl. Phys. A (2020). https://doi.org/10.1007/s00339-020-03664-6
62. P. Kumar, M. Chandra Mathpal, J. Prakash, B.C. Viljoen, W.D. Roos, H.C. Swart, Band gap tailoring of cauliflower-shaped CuO nanostructures by Zn doping for antibacterial applications. J. Alloys Compd. **832**, 154968 (2020)
63. S. Vasantharaj, S. Sathiyavimal, M. Saravanan, P. Senthilkumar, K. Gnanasekaran, M. Shanmugavel, Synthesis of ecofriendly copper oxide nanoparticles for fabrication over textile fabrics: characterization of antibacterial activity and dye degradation potential. J. Photochem. Photobiol. B Biol. **191**, 143–149 (2019)
64. J. Iqbal, T. Jan, S. Ul-Hassan, I. Ahmed, Q. Mansoor, M. Umair Ali, F. Abbas, M. Ismail, Facile synthesis of Zn doped CuO hierarchical nanostructures: Structural, optical and antibacterial properties. AIP Adv. **5**, 127112 (2015)
65. C. Parvathiraja, S. Shailajha, Bioproduction of CuO and Ag/CuO heterogeneous photocatalysis-photocatalytic dye degradation and biological activities. Appl. Nanosci. **11**, 1411–1425 (2021)
66. D.-N. Phan, N. Dorjjugder, Y. Saito, M. Qamar-Khan, P. Hajipour, A. Bahrami, A. Eslami, A. Hosseini-Abari, H.R.H. Ranjbar, Chemical bath synthesis of CuO-GO-Ag nanocomposites with enhanced antibacterial properties. J. Alloy. Compd. **821**, 153456 (2020)
67. E.H. Lacerda, F.C. Monteiro, J.R. Kloss, S.T. Fujiwara, Bentonite clay modified with Nb_2O_5: An efficient and reused photocatalyst for the degradation of reactive textile dye. J. Photochem. Photobiol. A Chem. **388**, 112084 (2019)
68. C.L. Ücker, V. Goetzke, S.R. Almeida, E.C. Moreira, M.M. Ferrer, P.L. Jardim, M.L. Moreira, C.W. Raubach, S. Cava, Photocatalytic degradation of rhodamine B using Nb_2O_5 synthesized with different niobium precursors: factorial design of experiments. Ceram. Int. **47**, 7889–7905 (2021)
69. M. Ponnar, C. Thangamani, P. Monisha, S.S. Gomathi, K. Pushpanathana, Influence of Ce doping on CuO nanoparticles synthesized by microwave irradiation method. Appl. Surf. Sci. **449**, 132–143 (2018)
70. R. Saravanan, S. Karthikeyan, V.K. Gupta, G. Sekaran, V. Narayanan, Stephen, Enhanced photocatalytic activity of ZnO/CuO nanocomposite for the degradation of textile dye on visible light illumination. Mater. Sci. Eng., C **33**, 91–98 (2013)
71. K. Velsankar, R.M. Aswin Kumar, R. Preethi, V. Muthulakshmi, S. Sudhahar, Green synthesis of CuO nanoparticles via Allium sativum extract and its characterizations on antimicrobial, antioxidant, antilarvicidal activities. J. Environ. Chem. Eng. **8**, 104123 (2020)
72. A. Pramothkumar, N. Senthilkumar, K.C. Mercy Gnana Malar, M. Meena, I. Vetha Potheher, comparative analysis on the dye degradation efficiency of pure Co, Ni and Mn-doped CuO nanoparticles. J. Mater. Sci. Mater Electr. **30**, 19043–19059 (2019)
73. A. Azam, A.S. Ahmed, M. Oves, M.S. Khan, S.S. Habib, A. Memic, Antimicrobial activity of metal oxide nanoparticles against Gram-positive and Gra negative bacteria: A comparative study. Int. J. Nanomed. **7**, 6003–6009 (2012)
74. S.M. Dizaj, F. Lotfipour, M. Barzegar-Jalali, M. Hossein Zarrintan, K. Adibkia, Antimicrobial activity of the metals and metal oxide nanoparticles. Mater. Sci. Eng. C **44**, 278–284 (2014)
75. M. Ahamed, H.A. Alhadlaq, M.M. Khan, P. Karuppiah, N.A. Al-Dhabi, Synthesis, characterization, and antimicrobial activity of copper oxide nanoparticles. J. Nanomater. **14**, 1–4 (2014)
76. I. Sondi, B. Salopek-Sondi, J Colloid Interface Sci **275**, 177–182 (2004)
77. K. Delgado, R. Quijada, R. Palma, H. Palza, Lett Appl Microbiol **53**, 50–54 (2011)
78. S. Rtimi, M.K.S. Ballo, D. Laub, C. Pulgarin, J.M. Entenza, A. Bizzini, R. Sanjines, J. Kiwi, Appl. Catal. A **498**, 185–191 (2015)
79. A. Azam, A.S. Ahmed, M. Oves, M.S. Khan, A. Memic, Int. J. Nanomed. **7**, 3527–3535 (2012)
80. S. Ramya, G. Viruthagiri, R. Gobi, N. Shanmugam, N. Kannadasan, Synthesis and characterization of Ni^{2+} ions incorporated CuO nanoparticles and its application in antibacterial activity. J. Mater. Sci.: Mater. Electron. **27**, 2701–2711 (2015)
81. M.J. Hajipour, K.M. Fromm, A.A. Ashkarran, D.J. de Aberasturi, I.R. de Larramendi, T. Rojo, V. Serpooshan, W.J. Parak, M. Mahmoudi, Erratum: antibacterial properties of nanoparticles. Trends Biotechnol. **30**, 499–511 (2012)

82. K.E. Rakesh, V. Rosy Antony, Photodegradation and antibacterial properties of zeolite cerium oxide nanocomposite. AIP Conf. Proc. **2162**, 020164 (2019)
83. K. Kannan, D. Radhika, M.P. Nikolova, V. Andal, K.K. Sadasivuni, L.S. Krishna, Facile microwave-assisted synthesis of metal oxide CdO-CuO nanocomposite: photocatalytic and antimicrobial enhancing properties. Optik. **218**, 165112 (2020)
84. S.A. Mohammed, L. Al Amouri, E. Yousif, A.A. Ali, H.F. Abbas, S. Alyaqoobi, Synthesis of NiO: V_2O_5 nanocomposite and its photocatalytic efficiency for methyl orange degradation. Heliyon. **4**, e00581 (2018)
85. D.M. Chethana, T.C. Thanuja, H.M. Mahesh, M.S. Kiruba, A.S. Jose, H.C. Barshilia, J. Manjanna, Synthesis structural, magnetic and NO_2 gas sensing property of CuO nanoparticles. Ceram. Int. **47**, 7 (2020)
86. O. Chamteut, S.W. Ji, Y. Cheong, G.J. Yim, Applicability of electrochemical wastewater treatment system powered by temperature difference energy. J. Hazard. Mater. **18**, 30106–30107 (2018)
87. P. Hajipour, A. Bahrami, A. Eslami, A. Hosseini-Abari, H. Hagh Ranjbar, Chemical bath synthesis of CuO-GO-Ag Nano composites with enhanced antibacterial properties. J. Alloy. Compd. **821**, 153456 (2020)